Human natural killer cells prevent infectious mononucleosis features by targeting lytic epstein-barr virus infection

Chijioke, Obinna ; Müller, Anne ; Feederle, Regina ; Barros, Mario Henrique M ; Krieg, Carsten ; Emmel, Vanessa ; Marcenaro, Emanuela ; Leung, Carol S ; Antsiferova, Olga ; Landtwing, Vanessa ; Bossart, Walter ; Moretta, Alessandro ; Hassan, Rocio ; Boyman, Onur ; Niedobitek, Gerald ; Delecluse, Henri-Jacques ; Capaul, Riccarda ; Münz, Christian

Abstract: Primary infection with the human oncogenic Epstein-Barr virus (EBV) can result in infectious mononucleosis (IM), a self-limiting disease caused by massive lymphocyte expansion that predisposes for the development of distinct EBV-associated lymphomas. Why some individuals experience this symptomatic primary EBV infection, whereas the majority acquires the virus asymptomatically, remains unclear. Using a mouse model with reconstituted human immune system components, we show that depletion of human natural killer (NK) cells enhances IM symptoms and promotes EBV-associated tumorigenesis mainly because of a loss of immune control over lytic EBV infection. These data suggest that failure of innate immune control by human NK cells augments symptomatic lytic EBV infection, which drives lymphocyte expansion and predisposes for EBV-associated malignancies.

DOI: https://doi.org/10.1016/j.celrep.2013.11.041

Cell Reports
Report

Cell PRESS
Open ACCESS

Human Natural Killer Cells Prevent Infectious Mononucleosis Features by Targeting Lytic Epstein-Barr Virus Infection

Obinna Chijioke,[1] Anne Müller,[1] Regina Feederle,[2] Mario Henrique M. Barros,[3] Carsten Krieg,[4] Vanessa Emmel,[5] Emanuela Marcenaro,[6,7] Carol S. Leung,[1] Olga Antsiferova,[1] Vanessa Landtwing,[1] Walter Bossart,[8] Alessandro Moretta,[6,7] Rocio Hassan,[5] Onur Boyman,[4] Gerald Niedobitek,[3] Henri-Jacques Delecluse,[2] Riccarda Capaul,[8] and Christian Münz[1,*]

[1]Department of Viral Immunobiology, Institute of Experimental Immunology, University of Zürich, 8057 Zürich, Switzerland
[2]DKFZ unit F100/INSERM unit U1074, 69120 Heidelberg, Germany
[3]Institute for Pathology, Unfallkrankenhaus Berlin, 12683 Berlin, Germany
[4]Laboratory of Applied Immunobiology, University of Zürich, 8006 Zürich, Switzerland
[5]Bone Marrow Transplantation Center, Instituto Nacional de Cancer (INCA), 20231-130 Rio de Janeiro, Brazil
[6]Dipartimento di Medicina Sperimentale, Università degli Studi di Genova, 16147 Genova, Italy
[7]Centro di Eccellenza per le Ricerche Biomediche, Università degli Studi di Genova, 16147 Genova, Italy
[8]Institute of Medical Virology, University of Zürich, 8006 Zürich, Switzerland
*Correspondence: christian.muenz@uzh.ch
http://dx.doi.org/10.1016/j.celrep.2013.11.041

SUMMARY

Primary infection with the human oncogenic Epstein-Barr virus (EBV) can result in infectious mononucleosis (IM), a self-limiting disease caused by massive lymphocyte expansion that predisposes for the development of distinct EBV-associated lymphomas. Why some individuals experience this symptomatic primary EBV infection, whereas the majority acquires the virus asymptomatically, remains unclear. Using a mouse model with reconstituted human immune system components, we show that depletion of human natural killer (NK) cells enhances IM symptoms and promotes EBV-associated tumorigenesis mainly because of a loss of immune control over lytic EBV infection. These data suggest that failure of innate immune control by human NK cells augments symptomatic lytic EBV infection, which drives lymphocyte expansion and predisposes for EBV-associated malignancies.

INTRODUCTION

Epstein-Barr virus (EBV) is carried as a persistent infection by more than 90% of the human adult population (Young and Rickinson, 2004). Whereas most individuals acquire the virus asymptomatically, up to 10% develop infectious mononucleosis (IM), especially when primary infection is delayed into adolescence (Balfour et al., 2013; Kutok and Wang, 2006; Luzuriaga and Sullivan, 2010). This disease is accompanied by high EBV titers and massive lymphocytosis, primarily by EBV-specific $CD8^+$ T cells targeting viral antigens that are involved in infectious particle production, called lytic infection (Hislop et al., 2007; Odumade et al., 2012). During the first 5 years after resolution of IM symptoms an increased risk to develop EBV-associated classical Hodgkin lymphoma is observed (Hjalgrim et al., 2003). EBV viremia, possibly driving EBV-specific $CD8^+$ T cell expansion and tumorigenesis, could result from insufficient innate immune control of EBV, and indeed frequencies or counts for the innate lymphocytes natural killer (NK) cells were found to either inversely or directly correlate with EBV titers in infectious mononucleosis (Balfour et al., 2013; Williams et al., 2005). Further arguing for a role of NK cells in EBV-specific immune control, primary immunodeficiencies that affect NK cells or NK cell recognition of EBV-transformed B cells have been reported to be associated with EBV-positive malignancies and high susceptibility to EBV (Eidenschenk et al., 2006; Parolini et al., 2000; Shaw et al., 2012). Because experimental in vivo models for dissecting the pathogenesis of this human B cell tropic herpes virus or close relatives are rare (Melkus et al., 2006; Sashihara et al., 2011; Traggiai et al., 2004; Yajima et al., 2008), addressing and manipulating specific parameters of the immune response to EBV remained difficult. In order to characterize the role of NK cells during primary EBV infection, we investigated NOD-scid $\gamma_c^{-/-}$ mice with reconstituted human immune system components (huNSG mice), which constitute a suitable in vivo model for human NK cell responses and EBV infection as well as virus-specific immune control (Rämer et al., 2011; Shultz et al., 2010; Strowig et al., 2009, 2010; White et al., 2012; Yajima et al., 2009).

RESULTS

Human NK Cells Dampen Immunophenotype during EBV Infection

Human and mouse NK cells specifically express NKp46 (Pessino et al., 1998; Walzer et al., 2007), and the majority of human NK

cells of huNSG mice are positive for NKp46 as well (Strowig et al., 2010). Therefore, the NKp46-specific monoclonal antibody BAB281 was used for NK cell depletion. This treatment significantly diminished both $CD3^-NKp46^+$ and $CD3^-CD56^+$ cell populations in treated mice (Figures S1A and S1B), whereas an isotype control antibody neither altered the composition of the reconstituted human immune system compartments nor the course of infection (data not shown). Infection of huNSG mice via intraperitoneal inoculation with 1×10^5 Raji-infecting units (RIU) of B95-8 EBV resulted in increased $CD8^+$ T cells frequencies and total numbers in both spleen and blood over the 6-week course of infection (Figures 1A–1D). This characteristic feature of acute IM was significantly more pronounced in NK-cell-depleted animals (Figures 1A–1D) and was accompanied with nearly 10-fold elevated serum levels of IFN-γ (Figure 1E). Moreover, in animals depleted of human NK cells, IFN-γ mRNA expressed in $CD4^+$ T cells was also significantly increased, reaching expression similar to $CD8^+$ T cells in nondepleted animals after infection (Figures 1F and 1G). The splenomegaly, resulting from EBV-stimulated $CD8^+$ T cell expansion, was enhanced in the absence of NK cells (Figure 1H). Thus, prominent features of symptomatic primary EBV infection in humans, i.e., acute IM, can be modeled in huNSG mice and are strongly pronounced in animals depleted of human NK cells.

Human $CD8^+$ T Cells Display an Activated Memory Phenotype after EBV Infection

In order to characterize the IM-like T cell expansion after EBV infection of NK-cell-depleted huNSG mice further, we phenotyped their $CD4^+$ and $CD8^+$ T cells. Activated memory T cells were mainly found within the $CD8^+$ T cell compartment in infected animals (Figures S2A and S2B) and expanded at the cost of naive $CD8^+$ T cell frequencies with NK cell depletion significantly affecting CX3CR1 upregulation and expansion of $CD11a^+$ $CD127^-$ $CD8^+$ T cells, which in mice have been proposed to be short-lived effector cells (Kaech et al., 2003) (Figures S2C and S2D). Inhibitory receptors and terminal differentiation markers on $CD8^+$ T cells were also significantly upregulated upon EBV infection, exclusively on cells coexpressing the memory marker CD45RO (Figure S2E). Still $CD8^+$ T cells displayed high levels of the effector molecules perforin and granzyme B with the latter significantly more expressed in animals depleted of NK cells (Figure S2F). Despite this terminal differentiation phenotype of $CD8^+$ T cells during EBV infection of NK-cell-depleted mice, these $CD8^+$ T cells were still able to exert considerable control over viral titers in NK-cell-depleted animals, because $CD8^+$ T cell depletion on top of NK cell depletion led to one log increased viral loads in blood and spleen (Figures 1I and 1J; for depletion efficiency, see Figures S1C and S1D). Thus, a highly activated, but still protective, $CD8^+$ T cell phenotype that mimics the one seen in IM in humans (Hislop and Sabbah, 2008; Odumade et al., 2012) could be observed during EBV infection in huNSG mice, especially after human NK cell depletion.

EBV Infection Drives an Initial Expansion of the Human NK Cell Compartment

This NK-cell-mediated restriction of $CD8^+$ T cell expansion was associated with the accumulation of a distinct NK cell subset in peripheral blood. We observed on average 2-fold increased frequencies of NK cells (identified as $CD3^-NKp46^+$ cells unless otherwise stated) 4 weeks postinfection (Figures 2B and S3A), coinciding with increased CD16 expression on NK cells (Figure 2C). This NK cell expansion or enhanced recruitment to the blood was followed by a contraction of NK cell frequencies in both the periphery and spleen (Figures 2A, 2B, and S3A). Human NK cells 6 weeks postinfection did not significantly proliferate as indicated by staining for the proliferation marker Ki-67 (Figure S3B) as has been described for NK cells in human acute IM (Zhang et al., 2007) and only slightly upregulated the activation marker CD69 (Figure 2E) compared to the robust upregulation for both CD69 and Ki-67 on human $CD8^+$ T cells (Figures 2E and S3B, respectively). Frequencies of more differentiated $CD16^+$ NK cells were still elevated (Figure 2D), but the majority remained NKG2A positive and killer immunoglobulin-like receptor (KIR) negative (Figures 2E and 2F). Nevertheless, NK cells expressed less CD27 and a subset upregulated LIR-1 without increased expression of the terminal differentiation marker CD57 or NKG2C (Figures 2E and 2F; data not shown). Therefore, EBV infection drives an initial NK cell accumulation in the blood that precedes the peak of the T cell response as well as a virus-induced lasting differentiation to mostly $CD16^+NKG2A^+KIR^-$ NK cells, indicative of an early differentiation phenotype.

Human NK Cells Control Viral Load and Prevent EBV-Induced Malignancy

The functional relevance of this NK cell subset accumulation became apparent from the analysis of viral titers in animals depleted of human NK cells. NK cells control EBV infection in huNSG mice, because cell-associated viral titers in both spleen and blood were increased one log 5 to 6 weeks postinfection in the absence of NK cells (Figures 3A and 3B). Infected animals depleted of NK cells showed a dramatic loss of body weight (Figure 3C) as well as a significantly higher incidence of infiltrative lymphomatous tumors at multiple sites (Figures 3D–3K; Figure S4A), which were mostly monoclonal (Figures S4B–S4D) compared to infected nondepleted animals. However, when NK cells were further expanded and differentiated to express CD16, KIRs, and CD57 through cytokine-treatment driven expansion and differentiation, they controlled EBV infection less well (Figure S5). These data indicate that especially human NK cells with an early differentiation phenotype control viral load and prevent detrimental cancerous sequelae of infection in the host.

Human NK Cells Primarily Respond to Lytic EBV Infection

Given that, during IM primarily lytic EBV, antigen-specific $CD8^+$ T cells expand (Hislop et al., 2007), the differential regulation of latent, i.e., cell proliferation inducing, versus lytic viral replication by NK cells was analyzed. Intriguingly, viral copy numbers in plasma of NK-cell-depleted animals were more dramatically increased than in whole blood, up to 100-fold 5 and 6 weeks postinfection (Figure 4A). This led us to investigate whether signs of lytic infection were more readily observed in the absence of NK cells. Indeed, BZLF-1—one of the two

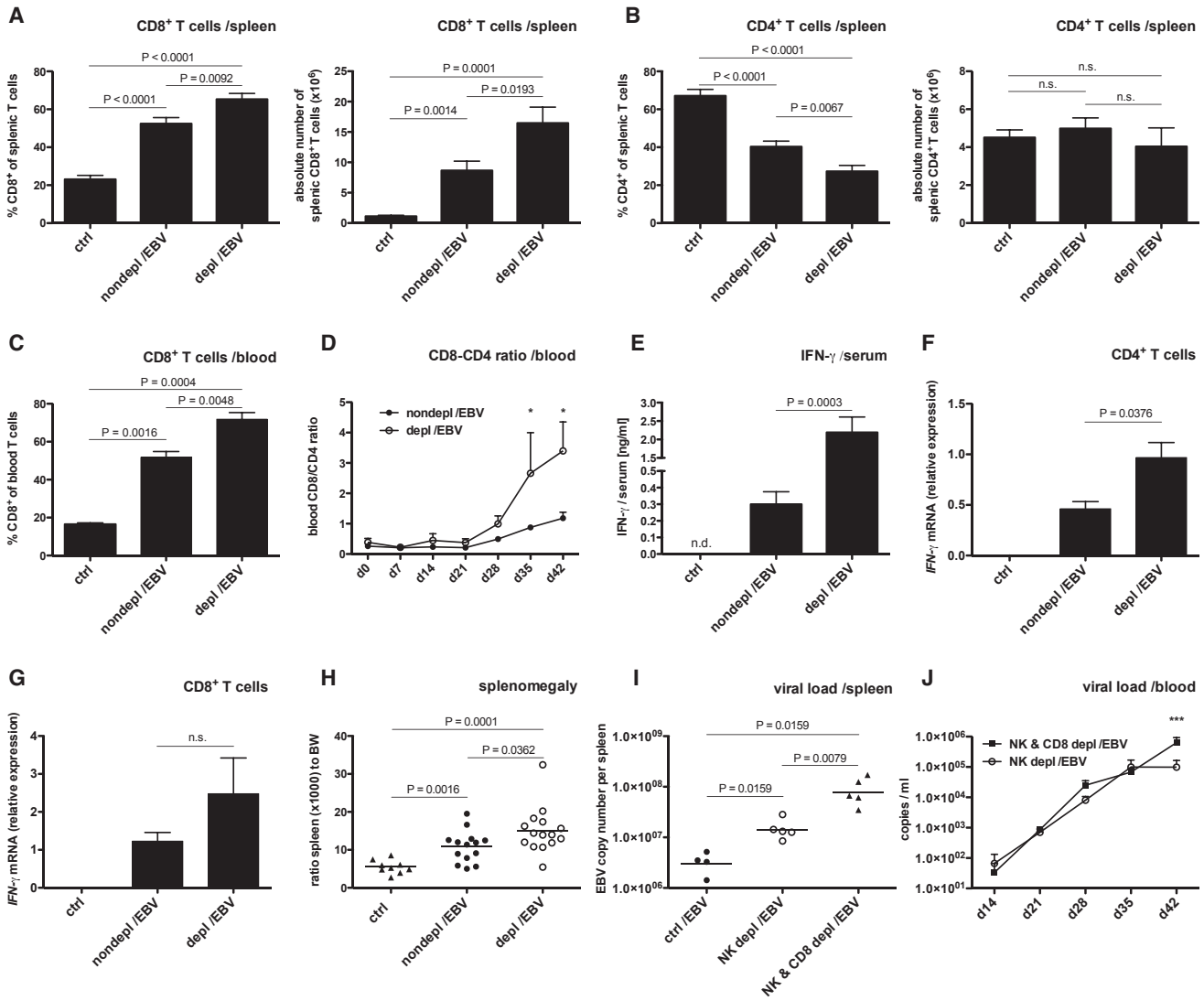

Figure 1. Human NK Cells Curb Human CD8$^+$ T Cell Expansion during EBV Infection

(A–D) Frequency and absolute numbers of CD8$^+$ T cells in spleen (A) and blood (C) 6 weeks after EBV infection in animals with (depl/EBV) and without (nondepl/EBV) NK cell depletion and in noninfected animals (ctrl). Frequency and absolute number of CD4$^+$ T cells in spleen six 6 weeks postinfection (p.i.) (B) and CD8-CD4 ratio over time p.i. in blood (D, *p < 0.05, two-way ANOVA with Bonferroni correction). CD4$^+$ and CD8$^+$ T cells were identified within live huCD45$^+$CD3$^+$ cells. n = 9–34, mean ± SEM.

(E) Concentration of human IFN-γ in serum 6 weeks p.i. in animals with and without NK cell depletion and in noninfected animals (n = 18, mean ± SEM).

(F and G) Relative expression of IFN-γ mRNA normalized to 18S in CD4$^+$ T cells (F) and CD8$^+$ T cells (G) sorted from splenocytes of noninfected animals (ctrl), from animals without (nondepl/EBV), and from animals with NK cell depletion (depl/EBV) 6 weeks after EBV infection. One representative experiment of three independent experiments is shown. n = 8, mean ± SEM.

(H) Ratio of spleen-to-body weight (BW) 6 weeks p.i. in animals with and without NK cell depletion and in noninfected animals (n = 38, bar represents mean). Data represent composite data from two to four independent experiments.

(I and J) Viral titers in spleen 6 weeks after EBV infection in animals without depletion (ctrl/EBV), animals depleted of NK cells (NK depl/EBV), and animals depleted of both NK and CD8$^+$ T cells (NK and CD8 depl/EBV) (I, n = 15, horizontal bar represents geometric mean, two-tailed Mann-Whitney test).

(J) Whole blood at various time points p.i. in animals depleted of both NK and CD8$^+$ T cells (NK & CD8 depl /EBV) and animals depleted of NK cells (NK depl /EBV) only (n = 10–13 per time point, mean ± SEM, ***p < 0.001, two-way ANOVA with Bonferroni correction). Data represent composite data from two independent experiments.

immediate early transactivators of EBV lytic cycle induction and indicator of lytic infection—and the late lytic antigen VCA p40 were expressed at increased levels in spleen sections from NK-cell-depleted animals (Figure 4B). Consistent with a higher availability of lytic EBV antigens, splenocytes of NK-cell depleted and infected animals recognized latently EBV-infected autologous B cell lines (LCLs) significantly less well by IFN-γ production than nondepleted controls (Figure 4C), and some

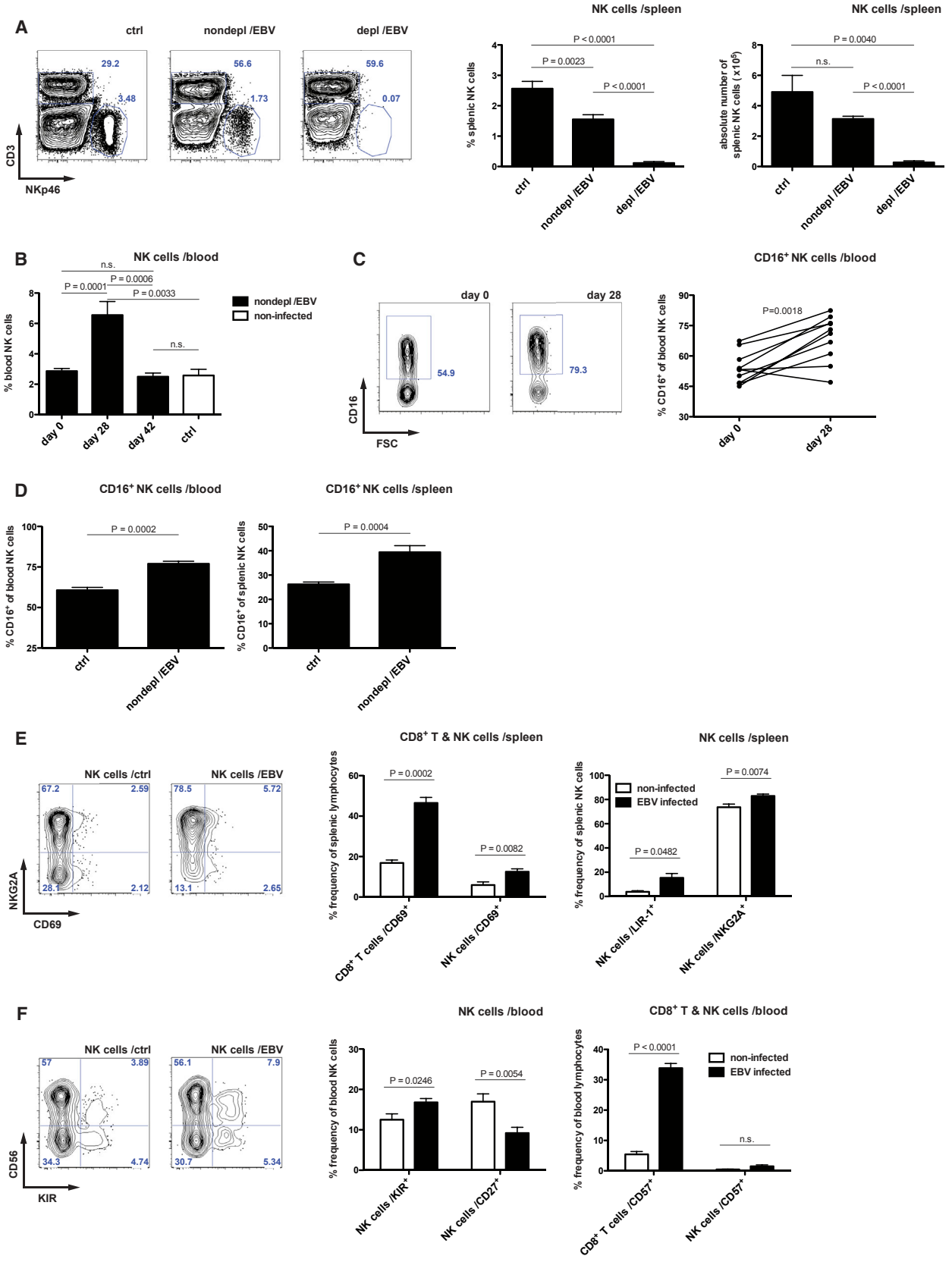

(legend on next page)

mice carried slightly elevated $CD8^+$ T cell populations that stained with MHC class I dextramers carrying lytic EBV antigen derived peptides (Figure S6). To confirm targeting of lytic infection by NK cells in vitro, we used AKBM cells that can be induced to enter the lytic cycle (Figure 4D). As reported, lytic AKBM cells showed decreased expression of MHC class I molecules (Pappworth et al., 2007) (Figure 4E) and as a surrogate for cytotoxicity elicited more degranulation of NK cells derived from EBV-infected animals than from latent AKBM cells (Figure 4F). This preferential recognition of lytically EBV-replicating B cells had been previously described for peripheral blood human NK cells in vitro (Pappworth et al., 2007). Altogether, these data suggest that NK cells preferentially respond to lytically infected cells, and one reason for this might be loss of inhibitory signals delivered by MHC class I molecules on the target cells.

Latent EBV Infection Is Unaffected by Human NK Cells

To test our hypothesis that NK cell preferentially restrict lytic EBV infection in vivo, we infected animals with 1×10^5 RIU BZLF-1 knockout (KO) B95-8 virus, which is unable to switch to lytic replication and therefore can only establish the default program of latent EBV infection. Indeed, no significant weight loss or difference in tumor formation was observed after KO virus infection, regardless of the presence or absence of NK cells (Figures 5A and 5B). Viral titers in spleen (Figure 5C) and whole blood (Figure 5D) were not significantly affected by NK cell depletion 6 weeks postinfection. In contrast, a revertant virus, in which BZLF-1 was reinserted into the BZLF-1 KO EBV, replicated to higher blood and splenic viral titers in the absence of NK cells (Figure S7), and therefore behaved similar to the wild-type virus infection. Interestingly, immunoactivation of the T cell compartment and development of splenomegaly after BZLF-1 KO EBV infection was almost similar to wild-type EBV infection for both NK-cell-depleted and nondepleted animals (Figure S8), confirming the potency of the KO virus. However, whereas a significant reduction of NK cells 6 weeks postinfection could still be observed in blood (Figures S9A and S9B), KO virus infection neither induced peripheral NK cell accumulation 4 weeks postinfection (Figure S9B), nor did it elicit increases in differentiated $CD16^+$ NK cells (Figures S9C and S9D). These results indicate an absence of protective NK cell responses to latent infection in vivo and establish lytic infection as the main stimulus for NK cell accumulation and differentiation.

DISCUSSION

Our study suggests that loss of NK-cell-mediated immune control over lytic EBV infection allows this human tumor virus to replicate to higher titers, driving lymphocytosis and promoting predisposition for EBV-associated lymphoma development. These are IM-like symptoms and known sequelae of IM (Hjalgrim et al., 2003), and the monoclonality of the emerging tumors as well as the associated weight loss argue for manifestations of fatal IM (Brown et al., 1986; Wick et al., 2002). NK cells might act only late during the course of infection in our model, because EBV first establishes default latent infection of B cells after intraperitoneal injection. Lytic replication is then only later reactivated from this latent pool to produce virus particles for increased B cell transformation and/or conditioning of the microenvironment for tumor growth (Hong et al., 2005; Ma et al., 2011). Only this delayed lytic replication seems to be restricted by human NK cells in huNSG mice. Such continuous contributions of NK cell responses to viral immune control, in addition to their role during early immune restriction of viruses, have also been suggested to form the basis for the selective NK cell subset expansions, seen during hantavirus, human immunodeficiency virus (HIV), chikungunya virus, and human cytomegalovirus (HCMV) infections (Björkström et al., 2011; Gumá et al., 2004; Hong et al., 2010; Lopez-Vergès et al., 2011; Petitdemange et al., 2011). These expansions might result from restimulation of NK cells with immunological memory features (Paust et al., 2010; Sun et al., 2009) or from recruitment of NK cell subsets to immune responses by memory $CD4^+$ T cells (Bihl et al., 2010; Horowitz et al., 2010). Our data support such a prolonged immune control by NK cells during viral infections and suggest that human NK cells of an early differentiation phenotype selectively restrict lytic EBV replication.

Instead of $CD8^+$ T cell expansion by elevated viral titers, caused by uncontrolled lytic replication, human T cell expansion could, however, also result from loss of direct NK cell cytotoxicity toward activated T cells, as has been suggested in mice (Lang et al., 2012; Waggoner et al., 2012). In favor of this interpretation, we also observed T cell expansion— albeit weaker—upon BZLF-1 knockout virus infection in NK-cell-depleted huNSG mice, without significant changes in EBV viremia. Therefore, NK cells might be involved in the prevention of IM by limiting viral antigen load that would otherwise drive massive T cell expansion and by restricting antiviral T cell expansion directly via cytotoxic restriction of activated T cells—in a possibly perforin-dependent

Figure 2. EBV Infection Drives an Initial Expansion and an Early Differentiation Phenotype of Human NK Cells

(A) Frequency and number of splenic NK cells 6 weeks after EBV infection in animals with (depl/EBV) and without (nondepl/EBV) NK cell depletion and in noninfected animals (ctrl), respectively, with representative plots. n = 22, mean ± SEM.

(B) Frequency of peripheral NK cells in nondepleted animals at day zero, day 28 p.i., day 42 p.i., and noninfected animals, respectively (n = 27, mean ± SEM).

(C) Expression of CD16 on peripheral NK cells in nondepleted EBV-infected animals at day zero and day 28 p.i. (n = 10), with representative staining for CD16 on pregated NK cells.

(D) Frequency of $CD16^+$ NK cells in blood and spleen 6 weeks p.i. in nondepleted animals (n = 9, mean ± SEM, one representative experiment for spleen).

(E and F) Expression of CD69 on splenic $CD8^+$ T cells and splenic NK cells, respectively, and frequency of $LIR\text{-}1^+$ and $NKG2A^+$ splenic NK cells 6 weeks p.i. with representative staining for NKG2A versus CD69 on pregated splenic NK cells 6 weeks p.i. (E). Frequency of KIR^+ and $CD27^+$ NK cells in peripheral blood with representative staining for CD56 versus KIR on pregated peripheral NK cells and frequency of $CD57^+$ peripheral $CD8^+$ T or NK cells, respectively, 6 weeks p.i. (F). NK cells were identified as $CD3^-NKp46^+$ cells within live $huCD45^+$ cells. n = 9–17, mean ± SEM. Data represent composite data from two to four independent experiments.

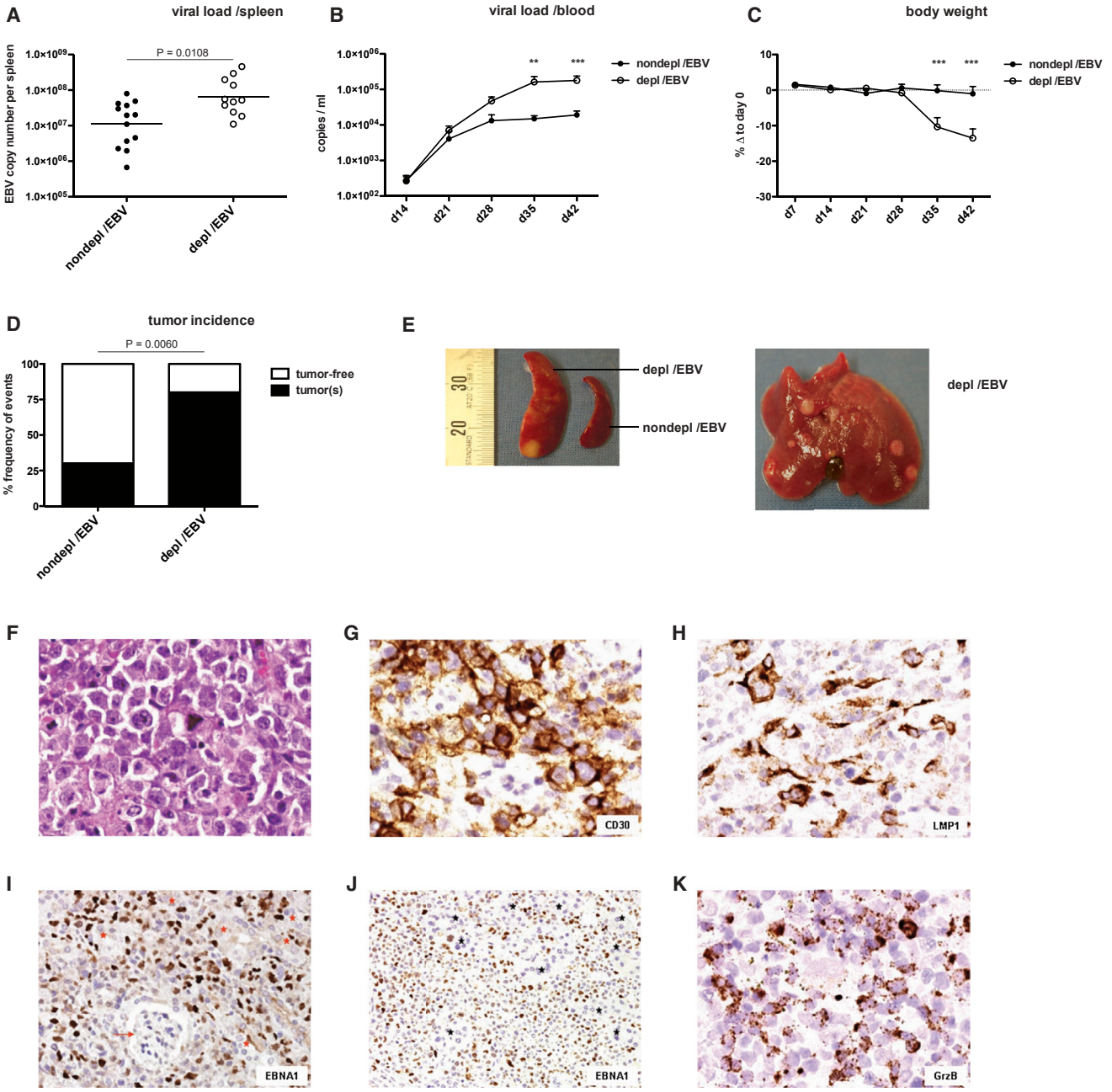

Figure 3. NK-Cell-Depleted Animals Develop Increased Viral Titers and Tumor Burden after EBV Infection

(A and B) Viral titers in spleen 6 weeks after EBV infection in animals with (depl/EBV) and without (nondepl/EBV) NK cell depletion (A, n = 24, horizontal bar represents geometric mean, two-tailed Mann-Whitney test) and whole blood at various time points p.i. (B, n = 21–26 per time point, mean ± SEM, $^{**}p < 0.01$, $^{***}p < 0.001$, two-way ANOVA with Bonferroni correction).

(C) Percent body weight loss after EBV infection in animals with and without NK cell depletion at various time points p.i. relative to day 0 (n = 15–26 per time point, mean ± SEM, $^{***}p < 0.001$, two-way ANOVA with Bonferroni correction).

(D) Incidence of all infiltrative tumors at multiple sites 6 weeks p.i. in animals with and without NK cell depletion (n = 36, Fisher's exact test for actual numbers). All data represent composite data from three to four independent experiments.

(E) Spleen with and without tumor formation from NK-cell-depleted or nondepleted animals 6 weeks p.i., respectively (left picture), and liver from NK-cell-depleted animal with multiple tumors (right picture).

(F–K) Tumor morphology.

(F–H) Pleomorphic immunoblasts, including occasional Reed-Sternberg like-cells (hematoxylin and eosin staining) (F) and (G), pleomorphic immunoblasts showing CD30 expression.

(legend continued on next page)

manner—as has been previously reported (Lang et al., 2012; Waggoner et al., 2012). These two scenarios do not need to be mutually exclusive but might indeed complement each other. Altogether, these data suggest that low NK cell reactivity—as shown for the association with increased cancer risk (Imai et al., 2000)—might identify EBV seronegative individuals at risk to develop IM, for which EBV vaccination could be developed.

EXPERIMENTAL PROCEDURES

Mice

NOD/LtSz-scid IL2Rγ^{null} (NOD-*scid* $\gamma_c^{-/-}$ or NSG) and HLA-A2 transgenic NSG (NSG-A2) mice were obtained from the Jackson Laboratory and bred and maintained at the Institute of Experimental Immunology, University of Zürich, under specific pathogen-free conditions. Newborn NSG mice (1 to 5 days old) were irradiated with 1 Gy using a Cs source. Five to six hours after irradiation, mice were injected intrahepatically with 1–2 × 10^5 $CD34^+$ human hematopoietic progenitor cells derived from human fetal liver tissue obtained from Advanced Bioscience Resources. Preparation of human fetal liver tissue and isolation of human $CD34^+$ cells was done as described previously (Strowig et al., 2009, 2010; White et al., 2012). Reconstitution of human immune system components in mice (huNSG) was analyzed 10–12 weeks after engraftment and again just before the start of the experiments. Mice with more than 60% reconstitution of $huCD45^+$ human immune system components in the lymphocytes of peripheral blood were used in the described experiments (average 85% $huCD45^+$ cells of peripheral blood lymphocytes, 30% $CD3^+$ T cells of human lymphocytes, 60% $CD19^+$ B cells of human lymphocytes, 3% NK cells of human lymphocytes, 80% $CD4^+$, and 20% $CD8^+$ T cells of human T cells), were of the NSG strain unless otherwise stated, were sex matched, and were 12–18 weeks old at the start of the experiments. All animal protocols were approved by the cantonal veterinary office of the canton of Zürich, Switzerland (protocol nos. 116/2008 and 148/2011). All studies involving human samples were reviewed and approved by the cantonal ethical committee of Zürich, Switzerland (protocol no. KEK-StV-Nr.19/08).

Virus Infection and NK and $CD8^+$ T Cell Depletion

GFP-Epstein-Barr virus (EBV) B95-8 wild-type, BZLF-1 KO, and BZLF-1 KO revertant were produced in 293 cells. Titration of viral concentrates was done on Raji cells in serial dilutions and calculated as Raji-infecting units (RIU) using flow cytometric analysis of GFP-positive Raji cells 2 days after infection of cells. HuNSG mice were infected via intraperitoneal injection of 1 × 10^5 RIUs with the respective viruses and followed for 6 weeks. Depletion of NK cells in huNSG mice was done via intraperitoneal injection of purified anti-NKp46 (clone BAB281) in PBS on three consecutive days (total of 300 μg per mouse). On the following day, depletion efficiency was determined in peripheral blood by flow cytometry (Figures S1A and S1B), and animals were infected by inoculation via intraperitoneal injection of 1 × 10^5 RIU EBV. $CD8^+$ T cells were depleted with purified anti-CD8 (clone OKT-8, Bio X Cell) diluted in PBS via intraperitoneal injection on three consecutive days (total of 150 μg per mouse) before infection and again 2 weeks postinfection every second day (50 μg per mouse each application).

Flow Cytometry

All fluorescently labeled antibodies were purchased from BD Biosciences, BioLegend, Invitrogen, and R&D Systems. Spleens were mechanically disrupted and filtered through a 70 μm cell strainer before separation of mononuclear cells on Ficoll-Paque gradients. Lysis of erythrocytes in whole blood was done with NH_4Cl. Dextramer staining was performed in accordance with the manufacturer's instructions (Immudex). For intracellular staining, the Cytofix/Cytoperm Kit from BD Biosciences was used. Cell suspensions were stained with antibodies for 30 min on ice, washed, and analyzed on FACSCanto or LSR Fortessa cytometers (BD Biosciences). Analysis of flow cytometric data was performed with FlowJo (Tree Star).

Quantification of Viral Load

Total DNA from whole blood or plasma was extracted using the QIAmp Mini Kit (Qiagen) in accordance with the manufacturer's instructions. Splenic tissue (5–15 mg) was processed using the QIAmp Tissue Kit (Qiagen) in accordance with the manufacturer's protocol. DNA was eluted in 50 μl Tris-EDTA and stored at 4°C. Quantitative analysis of EBV DNA was performed by a TaqMan (Applied Biosystems) real-time PCR technique as described previously (Berger et al., 2001) with modified primers for the BamHI W fragment (5′-CTTCTCAGTCCAGCGCGTTT-3′ and 5′-TCTAGGGAGGGGGACCACTG-3′) and the fluorogenic probe (5′-(FAM)-CGTAAGCCAGACAGCAGCCAATTGT CAG-(TAMRA)-3′). All PCRs were run on an ABI Prism 7700 Sequence Detector (Applied Biosystems) and samples analyzed in duplicates.

ELISA

Detection of human IFN-γ in serum from huNSG mice was performed with a human IFN-γ ELISA Kit (Mabtech) in accordance with the manufacturer's instructions.

Quantitative Real-Time PCR

Total RNA was extracted using the RNeasy Micro Kit (Qiagen) in accordance with the manufacturer's instructions. Complementary DNA was reverse transcribed using the GoScript Reverse Transcription System (Promega). Primers and probes were predesigned Taqman Gene Expression Assays (Applied Biosystems, IFN-γ: Hs00989291_m1 and 18S: Hs99999901_s1). Real-time PCR was performed on a CFX384 Touch Real-Time PCR Detection System (Bio-Rad) machine. All samples were run in triplicates and normalized using 18S expression level.

AKBM Cells and Degranulation Assay

EBV-positive AKBM cells that express GFP upon switch from latent to lytic EBV replication were induced to enter the lytic cycle after ligation with F(ab) IgG. BZLF-1 and HLA class I expression was monitored after intracellular staining for BZLF-1 (BZ-1, Santa Cruz Biotechnology) and surface staining for HLA-ABC (w6/32), respectively. For the degranulation assay, splenic cell suspensions and induced (lytic) or noninduced (latent) AKBM cells were cocultured at a ratio of 1:1 for 5 hr with addition of monensin after 1 hr, and NK cells were then analyzed for expression of the degranulation marker CD107a.

Statistical Analysis

All data were analyzed with a two-tailed Student's t test unless otherwise stated. A p value of < 0.05 was considered statistically significant. Statistical analysis and generation of graphs was performed with Prism software (GraphPad).

SUPPLEMENTAL INFORMATION

Supplemental Information includes Supplemental Experimental Procedures and nine figures and can be found with this article online at http://dx.doi.org/10.1016/j.celrep.2013.11.041.

AUTHOR CONTRIBUTIONS

O.C., A.M., M.H.M.B., G.N., C.S.L., R.H., C.K., V.E., and V.L. planned, performed, and analyzed experiments. O.A. produced recombinant EBV stocks. W.B. and R.C. quantified viral titers. R.F., E.M., A.M., O.B., and H.-J.D.

(H) EBV-infected cells with expression of LMP1. Original magnification, 400×.
(I and J) $EBNA1^+$ (brown nuclear staining) pleomorphic immunoblasts in tumor bearing kidney (I, arrow indicates glomerulus, and red stars indicate renal tubules) and pancreatic tumor (J, black stars indicate the pancreatic acini). Original magnification, 200×.
(K) Spleen infiltrated by large numbers of granzyme B^+ cells (original magnification, 400×). All tissue derived from animals 6 weeks p.i.

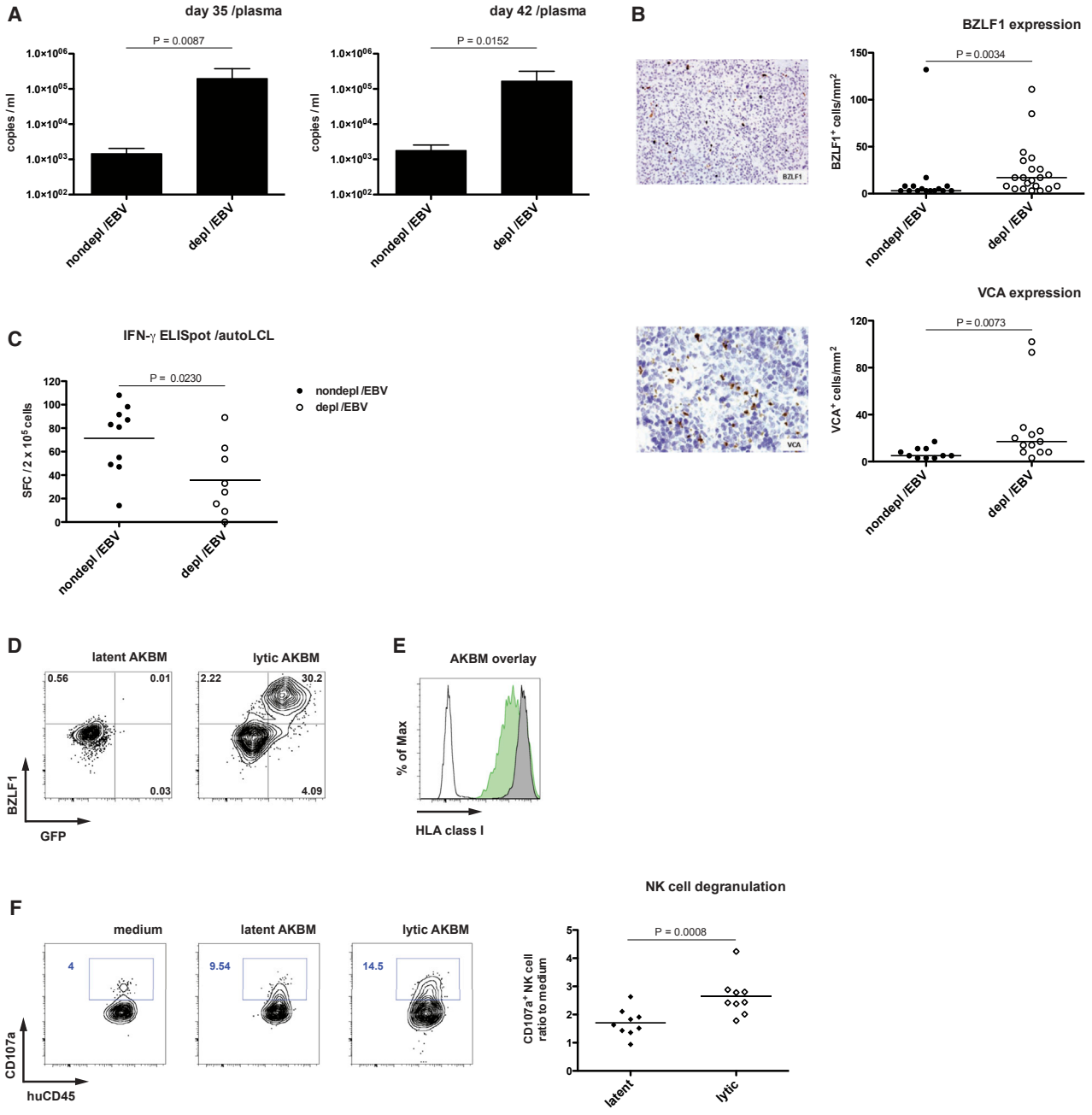

Figure 4. Loss of NK-Cell-Mediated Immune Control Augments Lytic EBV Infection

(A and B) EBV wild-type infection.

(A) EBV genome copies in plasma 5 and 6 weeks p.i. in animals with (depl/EBV) and without (nondepl/EBV) NK cell depletion (n = 11–12, mean ± SEM, two-tailed Mann-Whitney test).

(B) Staining for BZLF-1 (upper left, original magnification, 200×) and VCA (lower left, original magnification, 400×) in splenic sections from NK-cell-depleted animals 6 weeks p.i. with quantification of BZLF-1$^+$ cells per mm^2 in animals with and without NK cell depletion (upper right) and VCA$^+$ cells per mm^2 in animals with and without NK cell depletion (lower right), n = 23–36, horizontal bars represent median, two-tailed Mann-Whitney test.

(C) Functional assay (IFN-γ ELISpot) of ex vivo T cell response 6 weeks p.i. with autologous LCLs as targets and effector CD19$^+$ depleted splenic cells from animals with and without NK cell depletion (E:T = 5:1). n = 18, horizontal bar represents mean.

(D–F) Induction of lytic phase in AKBM cells and NK cell response. Staining for BZLF-1 in latent and lytic (induced) AKBM cells versus BMRF-1-driven GFP expression (D).

(E) HLA class I expression in latent and lytic AKBM cells (latent, gray graph; lytic, green graph; white graph, unstained control).

(F) Degranulation of pregated splenic NK cells from infected animals 6 weeks p.i. toward latent and lytic AKBM cells (n = 9, horizontal bar represents mean). All data represent composite data from at least two independent experiments.

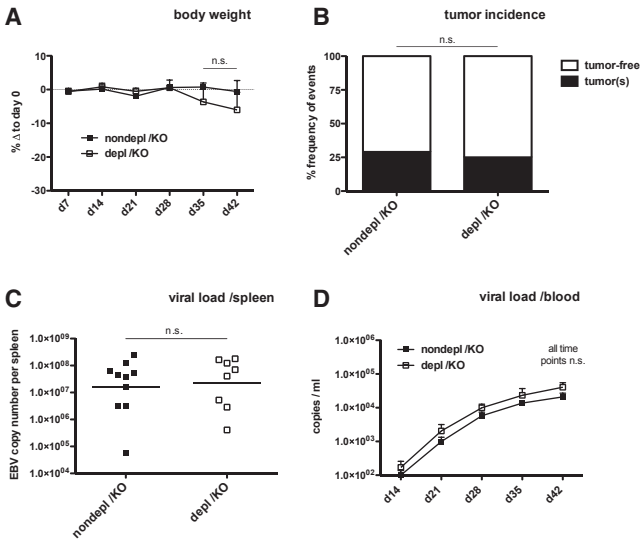

Figure 5. Latent EBV Infection Is Not Affected by Human NK Cells

(A–D) EBV BZLF-1 KO infection. Body weight loss after EBV BZLF-1 KO infection in animals with (depl/KO) and without (nondepl/KO) NK cell depletion at various time points p.i. (A, n = 12, mean ± SEM, two-way ANOVA with Bonferroni correction).

(B) Tumor incidence 6 weeks after EBV BZLF-1 KO infection in NK-cell-depleted and nondepleted animals (n = 15, Fisher's exact test for actual numbers).

(C and D) Viral titers in spleen 6 weeks p.i. (C, n = 18, horizontal bar represents geometric mean, two-tailed Mann-Whitney test) and blood at various time points p.i. (D, n = 12–18, mean ± SEM, *$p < 0.05$, two-way ANOVA with Bonferroni correction) in animals with and without NK cell depletion. All data represent composite data from at least two independent experiments.

provided crucial reagents. O.C. and C.M. designed the overall research and wrote the manuscript.

ACKNOWLEDGMENTS

We are grateful to Drs. Maike Ressing, Emmanuel Wiertz, and Martin Rowe for providing the AKBM cells and to Silvia Behnke of Sophistolabs for the histology in Figure S4. This work was supported by the National Cancer Institute (R01CA108609), the Sassella Foundation (10/02, 11/02, and 12/02), the Cancer Research Switzerland (KFS-02652-08-2010), the Association for International Cancer Research (11-0516), KFSP^{MS} and KFSP^{HLD} of the University of Zürich, the Vontobel Foundation, the Baugarten Foundation, the EMDO Foundation, the Sobek Foundation, the Foundation Acteria, Novartis, and the Swiss National Science Foundation (310030_143979 and CRSII3_136241) to C.M. R.H. is a fellow of the CNPq/INCT (Brazil; grants CNPq 481294/2009-0, 573806/2008-0, and FAPERJ - E-26/110.432/2010). M.H.MB. is supported by the Alexander von Humboldt Foundation. O.C. is the recipient of a postdoctoral fellowship of the Deutsche Forschungsgemeinschaft (CH 723/2-1).

Received: March 17, 2013
Revised: September 17, 2013
Accepted: November 25, 2013
Published: December 19, 2013

REFERENCES

Balfour, H.H., Jr., Odumade, O.A., Schmeling, D.O., Mullan, B.D., Ed, J.A., Knight, J.A., Vezina, H.E., Thomas, W., and Hogquist, K.A. (2013). Behavioral, virologic, and immunologic factors associated with acquisition and severity of primary Epstein-Barr virus infection in university students. J. Infect. Dis. *207*, 80–88.

Berger, C., Day, P., Meier, G., Zingg, W., Bossart, W., and Nadal, D. (2001). Dynamics of Epstein-Barr virus DNA levels in serum during EBV-associated disease. J. Med. Virol. *64*, 505–512.

Bihl, F., Pecheur, J., Bréart, B., Poupon, G., Cazareth, J., Julia, V., Glaichenhaus, N., and Braud, V.M. (2010). Primed antigen-specific CD4$^+$ T cells are required for NK cell activation in vivo upon Leishmania major infection. J. Immunol. *185*, 2174–2181.

Björkström, N.K., Lindgren, T., Stoltz, M., Fauriat, C., Braun, M., Evander, M., Michaëlsson, J., Malmberg, K.J., Klingström, J., Ahlm, C., and Ljunggren, H.G. (2011). Rapid expansion and long-term persistence of elevated NK cell numbers in humans infected with hantavirus. J. Exp. Med. *208*, 13–21.

Brown, N.A., Liu, C., Garcia, C.R., Wang, Y.F., Griffith, A., Sparkes, R.S., and Calame, K.L. (1986). Clonal origins of lymphoproliferative disease induced by Epstein-Barr virus. J. Virol. *58*, 975–978.

Eidenschenk, C., Dunne, J., Jouanguy, E., Fourlinnie, C., Gineau, L., Bacq, D., McMahon, C., Smith, O., Casanova, J.L., Abel, L., and Feighery, C. (2006). A novel primary immunodeficiency with specific natural-killer cell deficiency maps to the centromeric region of chromosome 8. Am. J. Hum. Genet. *78*, 721–727.

Gumá, M., Angulo, A., Vilches, C., Gómez-Lozano, N., Malats, N., and López-Botet, M. (2004). Imprint of human cytomegalovirus infection on the NK cell receptor repertoire. Blood *104*, 3664–3671.

Hislop, A.D., and Sabbah, S. (2008). CD8$^+$ T cell immunity to Epstein-Barr virus and Kaposi's sarcoma-associated herpes virus. Semin. Cancer Biol. *18*, 416–422.

Hislop, A.D., Taylor, G.S., Sauce, D., and Rickinson, A.B. (2007). Cellular responses to viral infection in humans: lessons from Epstein-Barr virus. Annu. Rev. Immunol. *25*, 587–617.

Hjalgrim, H., Askling, J., Rostgaard, K., Hamilton-Dutoit, S., Frisch, M., Zhang, J.S., Madsen, M., Rosdahl, N., Konradsen, H.B., Storm, H.H., and Melbye, M. (2003). Characteristics of Hodgkin's lymphoma after infectious mononucleosis. N. Engl. J. Med. *349*, 1324–1332.

Hong, G.K., Gulley, M.L., Feng, W.H., Delecluse, H.J., Holley-Guthrie, E., and Kenney, S.C. (2005). Epstein-Barr virus lytic infection contributes to lymphoproliferative disease in a SCID mouse model. J. Virol. *79*, 13993–14003.

Hong, H.S., Eberhard, J.M., Keudel, P., Bollmann, B.A., Ballmaier, M., Bhatnagar, N., Zielinska-Skowronek, M., Schmidt, R.E., and Meyer-Olson, D. (2010). HIV infection is associated with a preferential decline in less-differentiated CD56^{dim} CD16$^+$ NK cells. J. Virol. *84*, 1183–1188.

Horowitz, A., Newman, K.C., Evans, J.H., Korbel, D.S., Davis, D.M., and Riley, E.M. (2010). Cross-talk between T cells and NK cells generates rapid effector responses to Plasmodium falciparum-infected erythrocytes. J. Immunol. *184*, 6043–6052.

Imai, K., Matsuyama, S., Miyake, S., Suga, K., and Nakachi, K. (2000). Natural cytotoxic activity of peripheral-blood lymphocytes and cancer incidence: an 11-year follow-up study of a general population. Lancet *356*, 1795–1799.

Kaech, S.M., Tan, J.T., Wherry, E.J., Konieczny, B.T., Surh, C.D., and Ahmed, R. (2003). Selective expression of the interleukin 7 receptor identifies effector CD8 T cells that give rise to long-lived memory cells. Nat. Immunol. *4*, 1191–1198.

Kutok, J.L., and Wang, F. (2006). Spectrum of Epstein-Barr virus-associated diseases. Annu. Rev. Pathol. *1*, 375–404.

Lang, P.A., Lang, K.S., Xu, H.C., Grusdat, M., Parish, I.A., Recher, M., Elford, A.R., Dhanji, S., Shaabani, N., Tran, C.W., et al. (2012). Natural killer cell activation enhances immune pathology and promotes chronic infection by limiting CD8$^+$ T-cell immunity. Proc. Natl. Acad. Sci. USA *109*, 1210–1215.

Lopez-Vergès, S., Milush, J.M., Schwartz, B.S., Pando, M.J., Jarjoura, J., York, V.A., Houchins, J.P., Miller, S., Kang, S.M., Norris, P.J., et al. (2011). Expansion of a unique CD57$^+$NKG2Chi natural killer cell subset during acute human cytomegalovirus infection. Proc. Natl. Acad. Sci. USA *108*, 14725–14732.

Luzuriaga, K., and Sullivan, J.L. (2010). Infectious mononucleosis. N. Engl. J. Med. *362*, 1993–2000.

Ma, S.D., Hegde, S., Young, K.H., Sullivan, R., Rajesh, D., Zhou, Y., Jankowska-Gan, E., Burlingham, W.J., Sun, X., Gulley, M.L., et al. (2011). A new model of Epstein-Barr virus infection reveals an important role for early lytic viral protein expression in the development of lymphomas. J. Virol. *85*, 165–177.

Melkus, M.W., Estes, J.D., Padgett-Thomas, A., Gatlin, J., Denton, P.W., Othieno, F.A., Wege, A.K., Haase, A.T., and Garcia, J.V. (2006). Humanized mice mount specific adaptive and innate immune responses to EBV and TSST-1. Nat. Med. *12*, 1316–1322.

Odumade, O.A., Knight, J.A., Schmeling, D.O., Masopust, D., Balfour, H.H., Jr., and Hogquist, K.A. (2012). Primary Epstein-Barr virus infection does not erode preexisting $CD8^+$ T cell memory in humans. J. Exp. Med. *209*, 471–478.

Pappworth, I.Y., Wang, E.C., and Rowe, M. (2007). The switch from latent to productive infection in epstein-barr virus-infected B cells is associated with sensitization to NK cell killing. J. Virol. *81*, 474–482.

Parolini, S., Bottino, C., Falco, M., Augugliaro, R., Giliani, S., Franceschini, R., Ochs, H.D., Wolf, H., Bonnefoy, J.Y., Biassoni, R., et al. (2000). X-linked lymphoproliferative disease. 2B4 molecules displaying inhibitory rather than activating function are responsible for the inability of natural killer cells to kill Epstein-Barr virus-infected cells. J. Exp. Med. *192*, 337–346.

Paust, S., Gill, H.S., Wang, B.Z., Flynn, M.P., Moseman, E.A., Senman, B., Szczepanik, M., Telenti, A., Askenase, P.W., Compans, R.W., and von Andrian, U.H. (2010). Critical role for the chemokine receptor CXCR6 in NK cell-mediated antigen-specific memory of haptens and viruses. Nat. Immunol. *11*, 1127–1135.

Pessino, A., Sivori, S., Bottino, C., Malaspina, A., Morelli, L., Moretta, L., Biassoni, R., and Moretta, A. (1998). Molecular cloning of NKp46: a novel member of the immunoglobulin superfamily involved in triggering of natural cytotoxicity. J. Exp. Med. *188*, 953–960.

Petitdemange, C., Becquart, P., Wauquier, N., Béziat, V., Debré, P., Leroy, E.M., and Vieillard, V. (2011). Unconventional repertoire profile is imprinted during acute chikungunya infection for natural killer cells polarization toward cytotoxicity. PLoS Pathog. *7*, e1002268.

Rämer, P.C., Chijioke, O., Meixlsperger, S., Leung, C.S., and Münz, C. (2011). Mice with human immune system components as in vivo models for infections with human pathogens. Immunol. Cell Biol. *89*, 408–416.

Sashihara, J., Hoshino, Y., Bowman, J.J., Krogmann, T., Burbelo, P.D., Coffield, V.M., Kamrud, K., and Cohen, J.I. (2011). Soluble rhesus lymphocryptovirus gp350 protects against infection and reduces viral loads in animals that become infected with virus after challenge. PLoS Pathog. *7*, e1002308.

Shaw, R.K., Issekutz, A.C., Fraser, R., Schmit, P., Morash, B., Monaco-Shawver, L., Orange, J.S., and Fernandez, C.V. (2012). Bilateral adrenal EBV-associated smooth muscle tumors in a child with a natural killer cell deficiency. Blood *119*, 4009–4012.

Shultz, L.D., Saito, Y., Najima, Y., Tanaka, S., Ochi, T., Tomizawa, M., Doi, T., Sone, A., Suzuki, N., Fujiwara, H., et al. (2010). Generation of functional human T-cell subsets with HLA-restricted immune responses in HLA class I expressing NOD/SCID/IL2r gamma(^{null}) humanized mice. Proc. Natl. Acad. Sci. USA *107*, 13022–13027.

Strowig, T., Gurer, C., Ploss, A., Liu, Y.F., Arrey, F., Sashihara, J., Koo, G., Rice, C.M., Young, J.W., Chadburn, A., et al. (2009). Priming of protective T cell responses against virus-induced tumors in mice with human immune system components. J. Exp. Med. *206*, 1423–1434.

Strowig, T., Chijioke, O., Carrega, P., Arrey, F., Meixlsperger, S., Rämer, P.C., Ferlazzo, G., and Münz, C. (2010). Human NK cells of mice with reconstituted human immune system components require preactivation to acquire functional competence. Blood *116*, 4158–4167.

Sun, J.C., Beilke, J.N., and Lanier, L.L. (2009). Adaptive immune features of natural killer cells. Nature *457*, 557–561.

Traggiai, E., Chicha, L., Mazzucchelli, L., Bronz, L., Piffaretti, J.C., Lanzavecchia, A., and Manz, M.G. (2004). Development of a human adaptive immune system in cord blood cell-transplanted mice. Science *304*, 104–107.

Waggoner, S.N., Cornberg, M., Selin, L.K., and Welsh, R.M. (2012). Natural killer cells act as rheostats modulating antiviral T cells. Nature *481*, 394–398.

Walzer, T., Bléry, M., Chaix, J., Fuseri, N., Chasson, L., Robbins, S.H., Jaeger, S., André, P., Gauthier, L., Daniel, L., et al. (2007). Identification, activation, and selective in vivo ablation of mouse NK cells via NKp46. Proc. Natl. Acad. Sci. USA *104*, 3384–3389.

White, R.E., Rämer, P.C., Naresh, K.N., Meixlsperger, S., Pinaud, L., Rooney, C., Savoldo, B., Coutinho, R., Bödör, C., Gribben, J., et al. (2012). EBNA3B-deficient EBV promotes B cell lymphomagenesis in humanized mice and is found in human tumors. J. Clin. Invest. *122*, 1487–1502.

Wick, M.J., Woronzoff-Dashkoff, K.P., and McGlennen, R.C. (2002). The molecular characterization of fatal infectious mononucleosis. Am. J. Clin. Pathol. *117*, 582–588.

Williams, H., McAulay, K., Macsween, K.F., Gallacher, N.J., Higgins, C.D., Harrison, N., Swerdlow, A.J., and Crawford, D.H. (2005). The immune response to primary EBV infection: a role for natural killer cells. Br. J. Haematol. *129*, 266–274.

Yajima, M., Imadome, K., Nakagawa, A., Watanabe, S., Terashima, K., Nakamura, H., Ito, M., Shimizu, N., Honda, M., Yamamoto, N., and Fujiwara, S. (2008). A new humanized mouse model of Epstein-Barr virus infection that reproduces persistent infection, lymphoproliferative disorder, and cell-mediated and humoral immune responses. J. Infect. Dis. *198*, 673–682.

Yajima, M., Imadome, K., Nakagawa, A., Watanabe, S., Terashima, K., Nakamura, H., Ito, M., Shimizu, N., Yamamoto, N., and Fujiwara, S. (2009). T cell-mediated control of Epstein-Barr virus infection in humanized mice. J. Infect. Dis. *200*, 1611–1615.

Young, L.S., and Rickinson, A.B. (2004). Epstein-Barr virus: 40 years on. Nat. Rev. Cancer *4*, 757–768.

Zhang, Y., Wallace, D.L., de Lara, C.M., Ghattas, H., Asquith, B., Worth, A., Griffin, G.E., Taylor, G.P., Tough, D.F., Beverley, P.C., and Macallan, D.C. (2007). In vivo kinetics of human natural killer cells: the effects of ageing and acute and chronic viral infection. Immunology *121*, 258–265.

SUPPLEMENTAL INFORMATION

Human natural killer cells prevent infectious mononucleosis features by targeting lytic Epstein-Barr virus infection

Obinna Chijioke, Anne Müller, Regina Feederle, Mario Henrique M. Barros, Carsten Krieg, Vanessa Emmel, Emanuela Marcenaro, Carol S. Leung, Olga Antsiferova, Vanessa Landtwing, Walter Bossart, Alessandro Moretta, Rocio Hassan, Onur Boyman, Gerald Niedobitek, Henri-Jacques Delecluse, Riccarda Capaul and Christian Münz

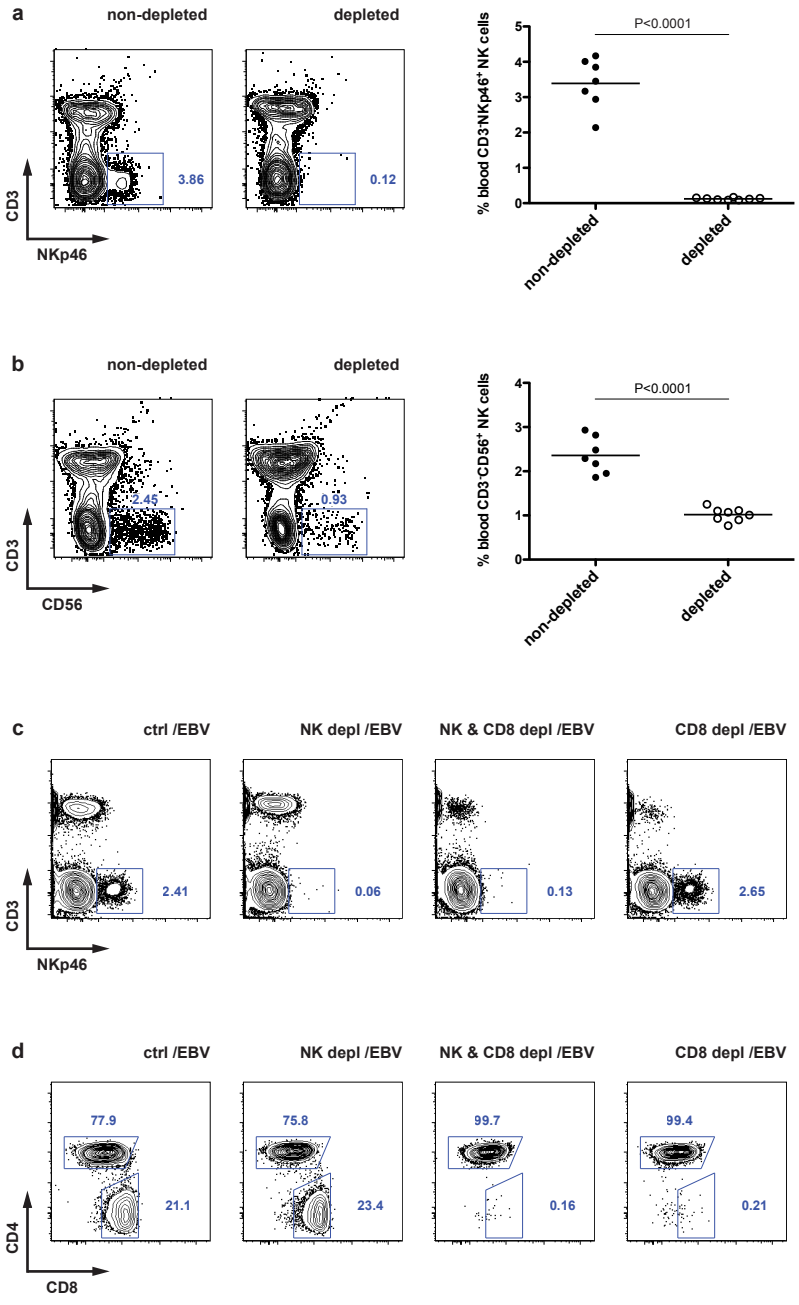

Figure S1
relates to Figure 1

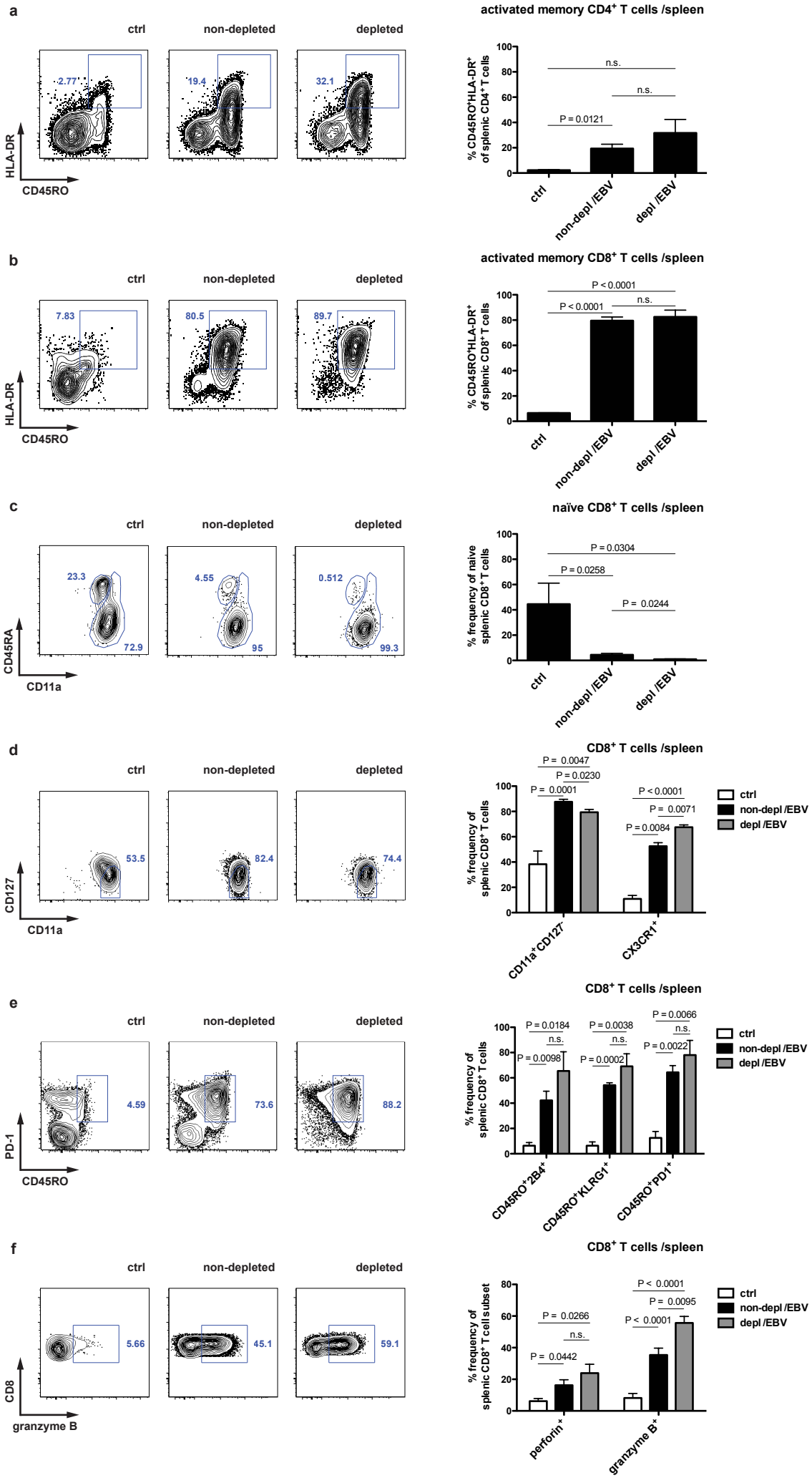

Figure S2
relates to Figure 1

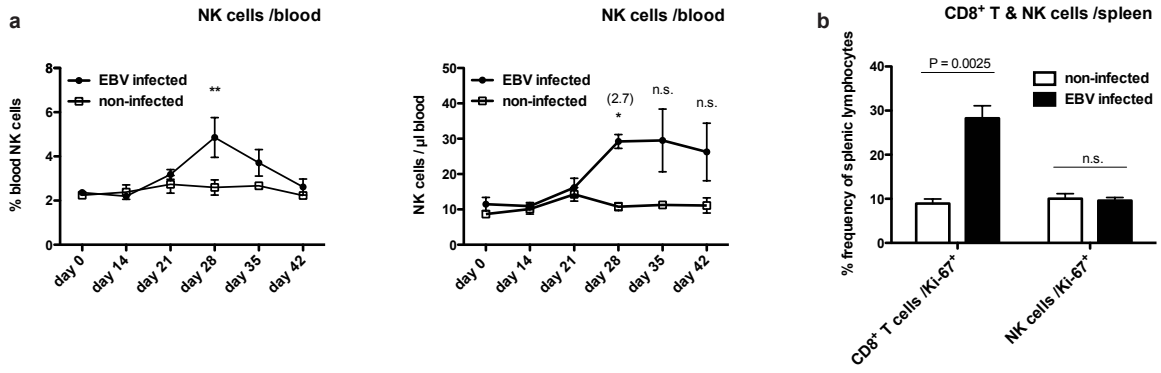

Figure S3
relates to Figure 2

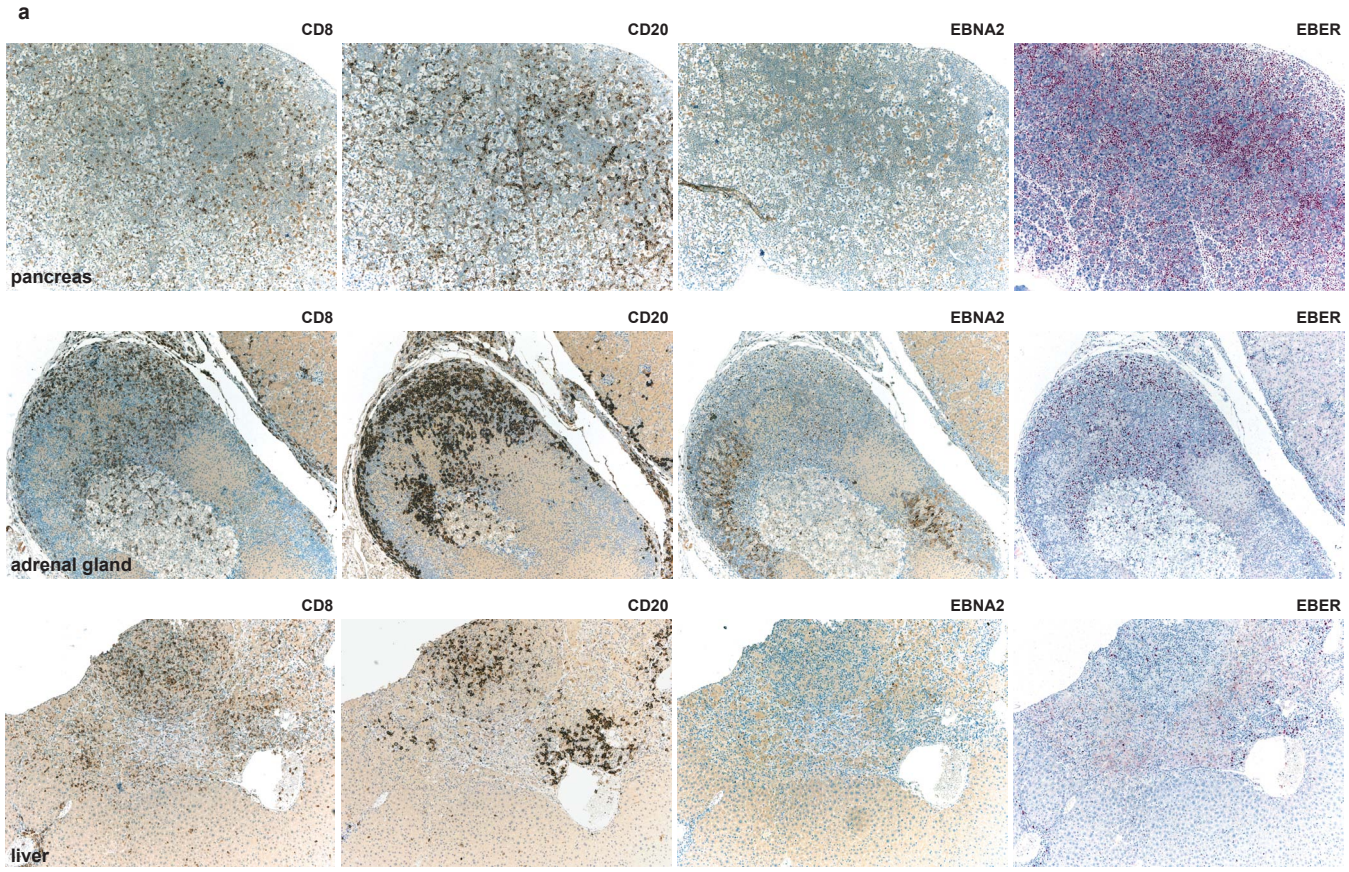

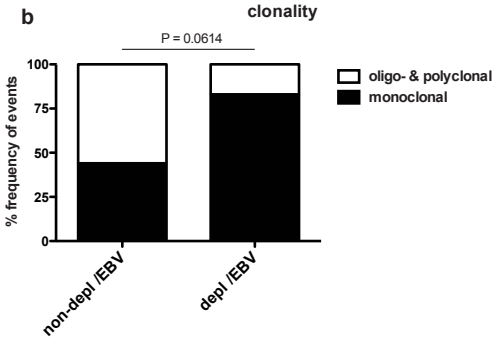

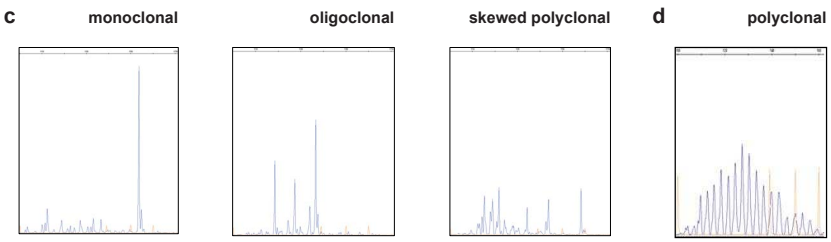

Figure S4
relates to Figure 3

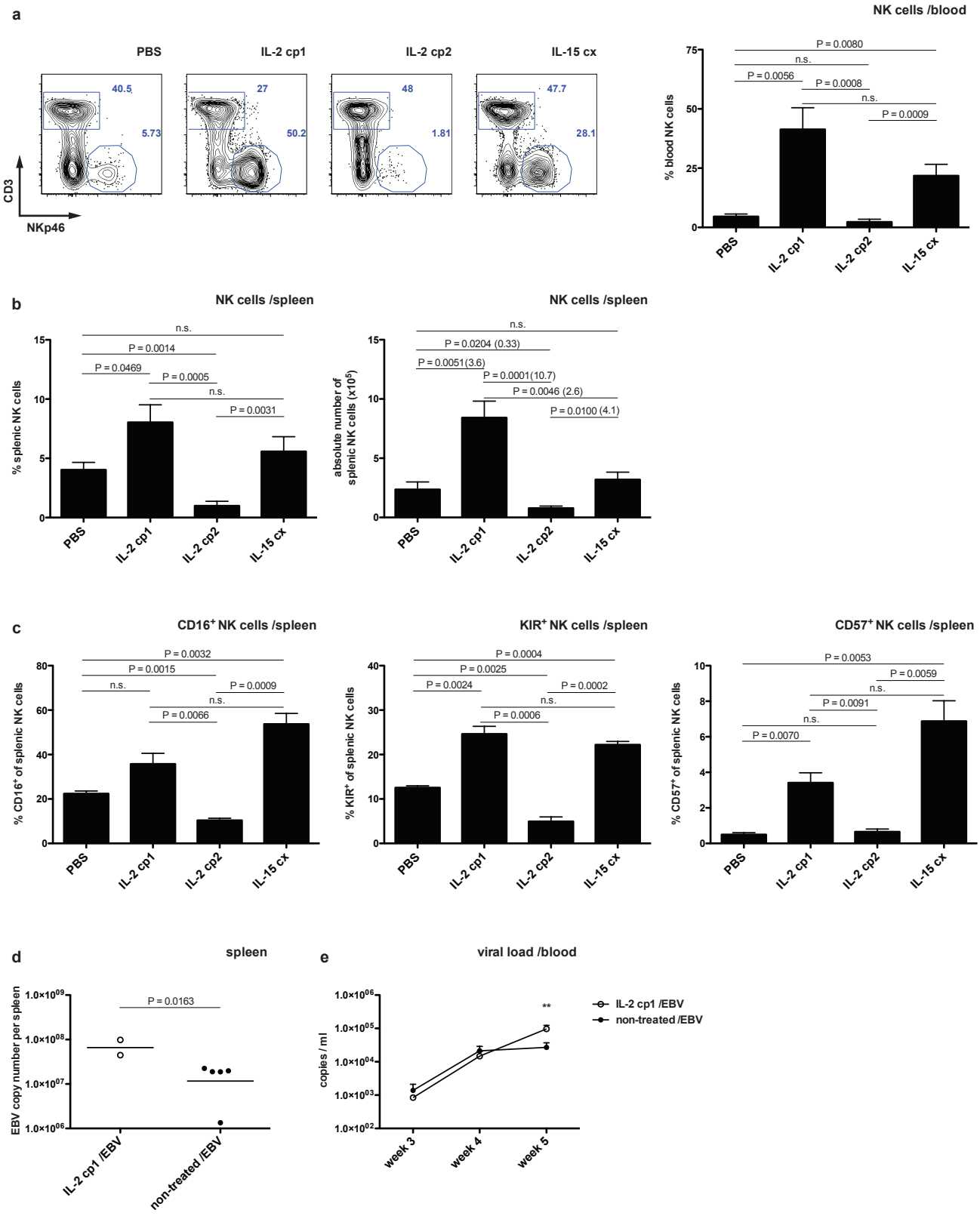

Figure S5

relates to Figure 3

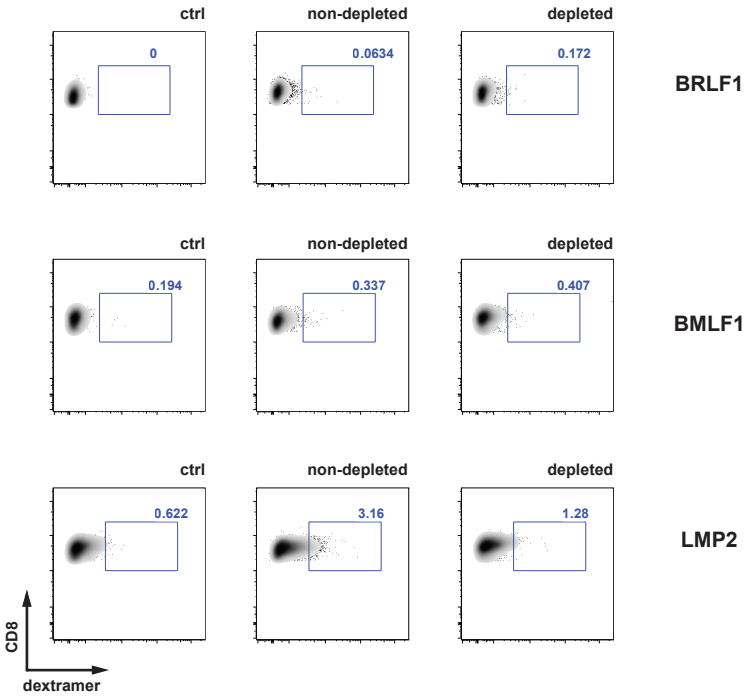

Figure S6
relates to Figure 4

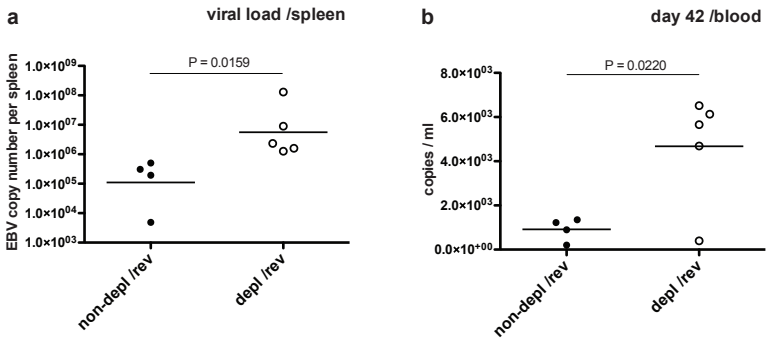

Figure S7

relates to Figure 4

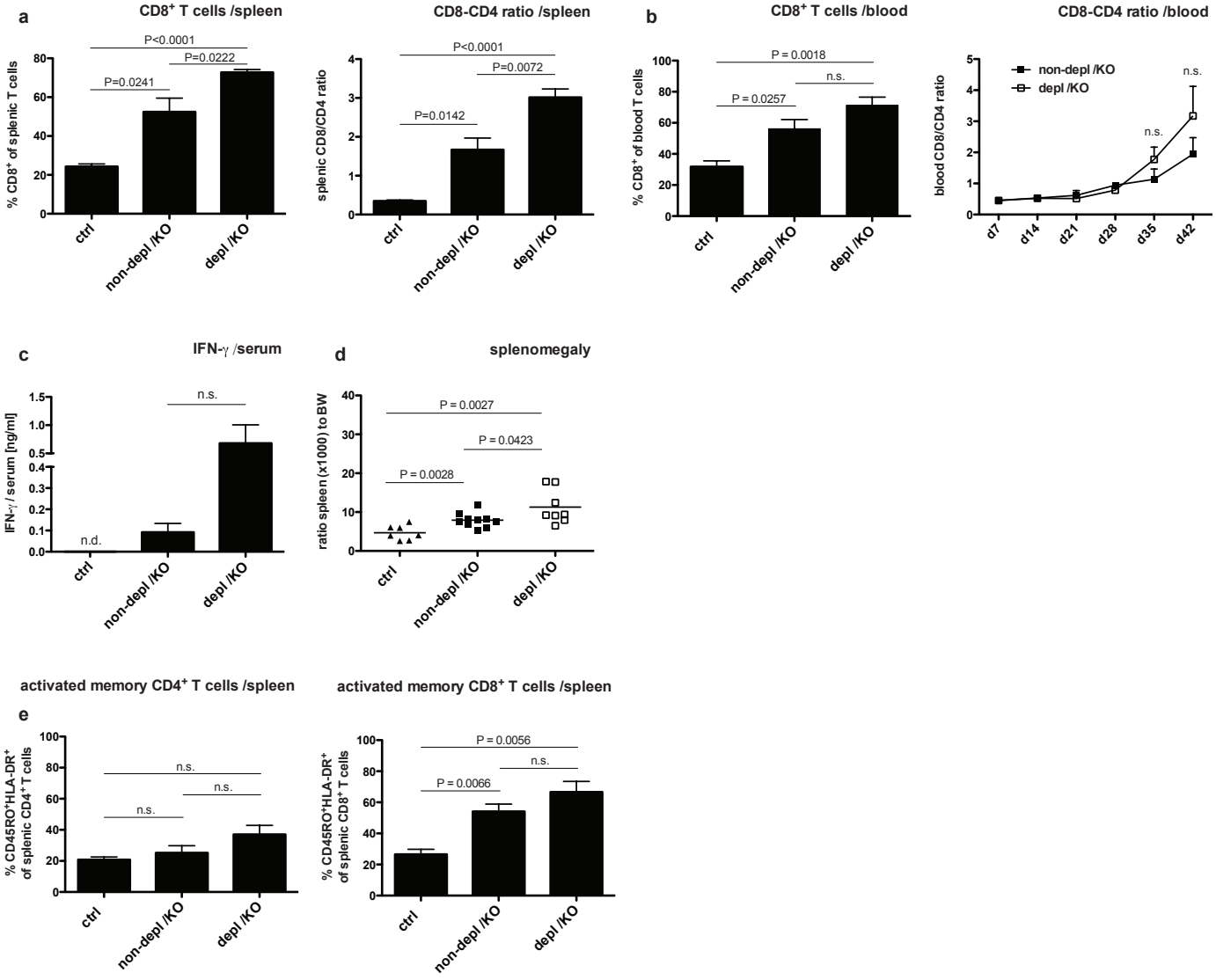

Figure S8
relates to Figure 5

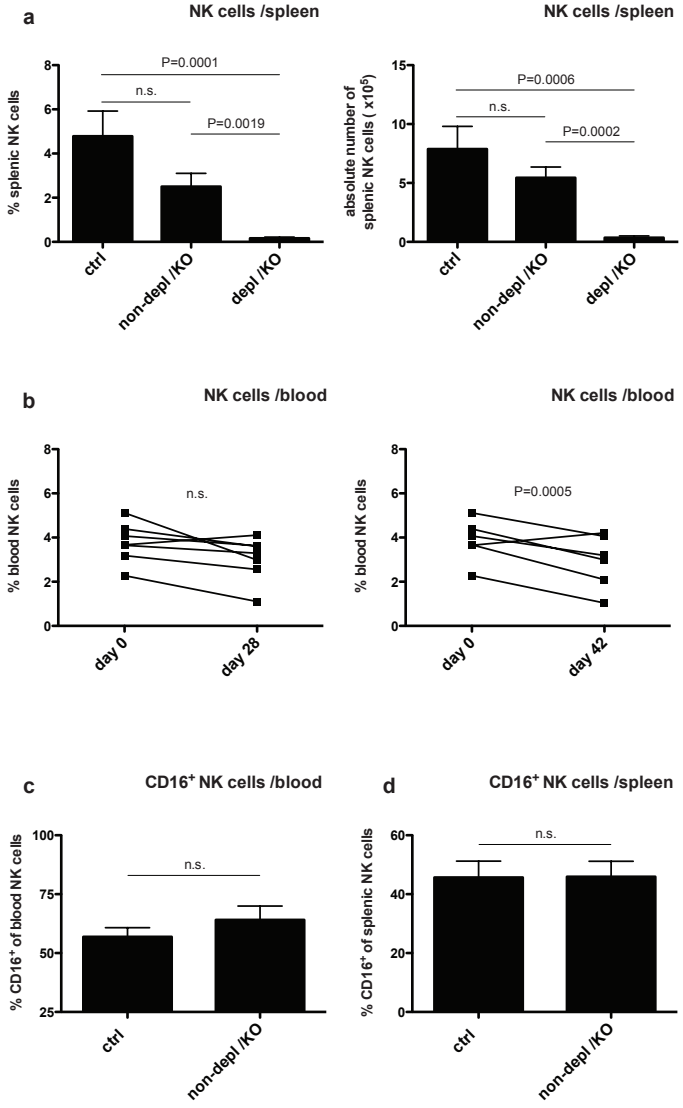

Figure S9
relates to Figure 5

SUPPLEMENTAL FIGURE LEGENDS

Figure S1: NKp46 specific antibodies efficiently deplete human NK cells and CD8 specific antibodies eliminate CD8$^+$ T cells in addition.

Human NK cells gated as CD3$^-$NKp46$^+$ - stained with clone 9E2 for NKp46 (**a**) or CD3$^-$ CD56$^+$ cells (**b**) in peripheral blood one day after depletion with a total of 300µg anti-NKp46 (clone BAB281) per animal for three consecutive days compared to control animals. Shown is one representative experiment of more than five independent experiments. n=15, horizontal bar represents mean. **c**-**d**, representative staining of NK cells (**c**, pregated on live huCD45$^+$ splenocytes within lymphocyte gate) and T cells (**d**, pregated on live huCD45$^+$CD3$^+$ splenocytes within lymphocyte gate) in animals without depletion (ctrl /EBV), animals depleted of NK cells (NK depl /EBV), animals depleted of both NK and CD8$^+$ T cells (NK & CD8 depl /EBV) and animals depleted of CD8$^+$ T cells (CD8 depl /EBV), respectively.

Figure S2: Phenotype of human memory T cells after EBV infection.

a-**b**, activated memory phenotype (CD45RO$^+$HLA-DR$^+$) splenic CD4$^+$ T cells with representative staining (**a**) or splenic CD8$^+$ T cells with representative staining (**b**) six weeks after EBV infection in animals with (depl /EBV) and without (non-depl /EBV) NK cell depletion and in non-infected animals (ctrl), respectively. Shown is one representative experiment of more than three independent experiments. n=14, mean ± s.e.m. **c**-**d**, naïve (CD45RA$^+$CD11a$^-$) splenic CD8$^+$ T cells with representative plots (**c**), effector cell phenotype (CD11a$^+$CD127$^-$) CD8$^+$ T cells in spleen and expression of CX3CR1 on splenic CD8$^+$ T cells six weeks p.i. with representative staining for CD127 and CD11a (**d**). n=9-18, mean ± s.e.m. **e**, frequency of CD45RO$^+$2B4$^+$, CD45RO$^+$KLRG1$^+$ and CD45RO$^+$PD-1$^+$ cells the CD8$^+$ T cell compartment with representative staining for CD45RO and PD-1 double positive CD8$^+$ T cells in the spleen six weeks after EBV infection, respectively, in animals with (depl /EBV) and

without NK cell depletion (non-depl /EBV) and in non-infected animals (ctrl). Shown is one representative experiment of two independent experiments. n=9, mean ± s.e.m. **f**, frequency of perforin$^+$ and granzyme B$^+$ splenic CD8$^+$ T cells six weeks p.i. with representative staining for granzyme B on pre-gated CD8$^+$ T cells. n=19-23, mean ± s.e.m. Data represent composite data from at least two independent experiments.

Figure S3: Peripheral NK cell accumulation peaks after 28 days of EBV infection.

a, kinetics of NK cell frequency and NK cell count per µl (fold difference to non-infected depicted in brackets) in peripheral blood in EBV infected animals and non-infected control animals at various time points p.i. (n=10, mean ± s.e.m., *P<0.05, **P<0.01, two-way analysis of variance (ANOVA) with Bonferroni correction, one representative experiment of more than two independent experiments is shown). **b,** frequency of splenic CD8$^+$ T cells or splenic NK cells expressing Ki-67$^+$ in EBV infected animals and non-infected control animals six weeks p.i., respectively. n=9-17, mean ± s.e.m. Data represent composite data from two independent experiments.

Figure S4: B cell lymphoproliferations of infected mice express EBV antigens and are mostly monoclonal in NK cell-depleted animals.

a-**b**, lymphoproliferative infiltration of pancreatic tissue, adrenal gland and liver immunostained for CD8, CD20, EBNA2 and virus-encoded RNA (EBER, in situ hybridization) in NK cell-depleted animals six weeks p.i. (original magnification, 100x). **b**-**d**, frequency of monoclonal and oligo-/polyclonal (with respect to immunoglobulin heavy chain gene rearrangements) lymphoproliferative lesions in EBV infected animals with (depl /EBV) and without NK cell depletion (non-depl /EBV) six weeks p.i. (**b**, n=21, χ^2 test for actual numbers) and representative electropherograms with monoclonal (left), oligoclonal (middle), skewed polyclonal (right) (**c**) and healthy

human PBMC control polyclonal pattern (**d**). Data represent composite data from samples from five independent experiments.

Figure S5: IL-2 or IL-15 cytokine formulations can boost NK cells in huNSG mice but drive terminal differentiation of NK cells.

a-**b**, frequency of NK cells in peripheral blood with representative staining (**a**) and frequency and absolute number of NK cells in spleen with fold difference shown in brackets (**b**) of huNSG mice after in vivo treatment with different cytokine formulations. n=23-24, mean ± s.e.m. Data represent composite data from two independent experiments. **c**, phenotype of splenic NK cells after in vivo treatment with different cytokine formulations with respect to CD16, KIR and CD57 expression, respectively. n=12, mean ± s.e.m., shown is one representative experiment of two independent experiments. **d**-**e**, EBV viral load in IL-2 compound 1 treated EBV infected animals (IL-2 cp1 /EBV) and mock treated EBV infected animals (non-treated /EBV) in spleen 5 weeks p.i. (**d**, n=7, horizontal bar represents geometric mean, two-tailed Mann Whitney test) and peripheral blood over time (**e**, n=7-10 per time point, mean ± s.e.m., **P<0.01, two-way analysis of variance (ANOVA) with Bonferroni correction). Experiment was terminated at 5 weeks p.i. due to animal loss in treatment group. Data from one representative experiment are shown.

Figure S6: Epitope-specific $CD8^+$ T cells are present after EBV infection.

Representative dextramer staining of pre-gated $CD8^+$ splenic T cells six weeks p.i. in huNSG-A2 mice with or without NK cell depletion and in non-infected animals (ctrl) for lytic (BRLF1 and BMLF1) and latent (LMP2) epitopes.

Figure S7: Infection with EBV BZLF-1 revertant recapitulates EBV wild-type infection.

a-**b**, EBV viral load in spleen (**a**, horizontal bar represents geometric mean, two-tailed Mann Whitney test) and peripheral blood six weeks p.i. (**b**, horizontal bar represents mean) in NK cell-depleted (depl /rev) or non-depleted (non-depl /rev) animals infected with EBV BZLF-1 revertant (rev) derived from EBV BZLF-1 KO. n=9. Data from one experiment are shown.

Figure S8: Ameliorated $CD8^+$ T cell expansion after EBV BZLF-1 KO infection.

a-**e**, EBV BZLF-1 infection in huNSG mice. Frequency of $CD8^+$ T cells and CD8-CD4 ratio six weeks p.i. in spleen in animals with (depl /KO) and without NK cell depletion (non-depl /KO) and in non-infected animals (ctrl) (**a**) and blood six weeks p.i. and over time after EBV BZLF-1 KO infection, respectively, in animals with and without NK cell depletion. (**b**). n=6-13, mean ± s.e.m. **c**, concentration of human IFN-γ in serum six weeks p.i. in animals with and without NK cell depletion and in non-infected animals (n=13, mean ± s.e.m.). **d**, ratio spleen to body weight (BW) six weeks p.i. in animals with and without NK cell depletion and in non-infected animals; n=25, horizontal bar represents mean. **e**, activated memory $CD45RO^+HLA\text{-}DR^+$ splenic $CD4^+$ T cells and splenic $CD8^+$ T cells, respectively, six weeks p.i. in animals with and without NK cell depletion and in non-infected animals (n=13, mean ± s.e.m.). All data represent composite data from at least two independent experiments.

Figure S9: Human NK cells do not significantly expand after EBV BZLF-1 KO infection.

a, frequency and number of splenic NK cells six weeks after EBV BZLF-1 KO infection in animals with (depl /KO) and without NK cell depletion (non-depl /KO) and in non-infected animals (ctrl). n=13, mean ± s.e.m. **b**, frequencies of peripheral NK cells day zero to day 28 and day zero to day 42, respectively, after EBV BZLF-1 KO infection. n=6-7. **c**-**d**, frequency of $CD16^+$ NK cells in blood (**c**) and spleen (**d**) in non-infected

(ctrl) and BZLF-1 KO infected (non-depl /KO) animals six weeks p.i. (n=8-9, mean ± s.e.m.). All data represent composite data from two independent experiments.

SUPPLEMENTAL EXPERIMENTAL PROCEDURES

Histology and immunohistochemistry

Tissue was fixed in 10% saline buffered formalin and paraffin embedded. For immunohistochemistry, mouse and rabbit anti-human monoclonal antibodies (all from Dako or Zytomed) were used and 4 µm sections processed using standard procedures on a BOND-MAX automated immunohistochemistry system (Leica Microsystems) with appropriate positive and negative controls. Antibody against EBNA1 (clone 1H4) was a gift from Dr. Kremmer. To identify lytic virus infection, IHC with antibodies directed against the BZLF1 immediate early protein (clone BZ1, Santa Cruz) and against the EBV p40 protein of the VCA complex (clone OT41, kind gift from Prof. J. Middeldorp) was used. EBV infection was determined by in situ hybridization (ISH) with digoxigenin-conjugated probes for EBV-encoded RNAs (EBER-ISH) (Meyer et al., 2011) or an EBER-1 probe developed with alkaline phosphatase on a BOND-MAX automated system.

As described previously for quantitative evaluation of labeled cells (Barros et al., 2012), each tissue core was photographed using AxioCam MRc camera (Zeiss) at a 200x magnification. The numbers of labeled cells were determined per 1 mm^2 using the image analysis software HISTO (Biomas). The markers related to EBV infection and immune cells were quantified in the spleen and/or in the peri-pancreatic lymph nodes but not in extra-lymphatic tissues.

In both non-depleted and NK cell-depleted mice, marked proliferation of pleomorphic immunoblasts was observed. These immunoblasts were uninucleated, binucleated or multinucleated, sometimes resembling Hodgkin and Reed-Sternberg cells. These cells were $CD79a^+$, $CD20^+$, $Bcl2^+$, EBER-ISH^+, $EBNA1^+$, $EBNA2^+$ and $LMP1^+$. Atypical $CD30^+$ cells were frequently observed, but numbers were not different between the two groups of animals. In all mice from both groups, liver, pancreas,

intestine, kidney, and/or peri-visceral fat showed infiltration of polymorphic EBV^+ immunoblasts, ranging from focal to diffuse, often associated with necrosis.

Analysis of clonality

DNA was extracted from 5 µm-sections of paraffin embedded tissue, following strict measures for avoiding cross-contamination between samples as described (Stefanoff et al., 2003). DNA was quantified using a Nanodrop® spectrophotometer and approximately 100 ng of DNA was used for PCR testing. All samples were shown to be PCR amplifiable for a human constitutive gene (β-globin) and an EBV specific gene (EBNA3C). B-cell clonality was investigated by PCR amplifications of immunoglobulin heavy chain (IGH) and light chain (IG kappa) gene rearrangements. T-cell clonality was ruled out by PCRs for TCR gamma rearrangements. Samples were assayed by multiplex PCR reactions using Biomed-2 FR3, FR2 and JH primers (IGH rearrangements) as well as Vk, Jk, Kde and INS primers (IG kappa rearrangements) (van Dongen et al., 2003), Cl_2Mg 1.5 Mm and 1U Platinum® Taq DNA polymerase (Invitrogen). PCR thermal profile consisted of an initial cycle of 95ºC at 5 min, followed by 35 cycles of 93ºC 45 sec, 60ºC 45 sec and 72ºC 90 sec. As post-PCR step, heteroduplex formation was promoted by denaturing PCR products at 94°C for 5 min followed by renaturation at 4ºC for 60 min. Products were electrophoresed in 8% non-denaturing polyacrylamide gels and silver stained. For fluorescent detection, the same procedures were performed, using 6'FAM-labeled JH primers. PCR products (1 µl) were mixed with 9.5 µl Hi-Di formamide, and 0.5 µl of LIZ fluorescent internal size standard. Electrophoresis was performed in a capillary sequencer 3130XL (Applied Biosystems) with POP7 polymer. Analysis was performed with the GeneMapper version 4.0 software.

To determine the clonality of a PCR product, a peak-height ratio was calculated as the ratio of peak heights between a 'clonal' prominent peak and the average of the two adjacent peaks. A PCR product was defined as monoclonal in the case of 1–2 sharp

peaks yielding a peak-height ratio >2. An oligoclonal pattern was defined as a non-Gaussian distribution of three or more prominent peaks. Polyclonality was defined in the presence of multiple peaks with a Gaussian distribution. Multiple peaks with a non-Gaussian distribution were classified as skewed polyclonal. All results were confirmed in the same sample on two repeated runs.

Cytokine treatment

Cytokine treatment with IL-2 formulations (compound 1 and compound 2) or IL-15 complexes was done i.p. with a total of 75000 I.U. over five consecutive days as described (Krieg et al., 2010) and analysis one day after the last treatment or infection with EBV for IL-2 compound 1.

SUPPLEMENTAL REFERENCES

Barros, M.H., Vera-Lozada, G., Soares, F.A., Niedobitek, G., and Hassan, R. (2012). Tumor microenvironment composition in pediatric classical Hodgkin lymphoma is modulated by age and Epstein-Barr virus infection. Int J Cancer *131*, 1142-1152.

Krieg, C., Letourneau, S., Pantaleo, G., and Boyman, O. (2010). Improved IL-2 immunotherapy by selective stimulation of IL-2 receptors on lymphocytes and endothelial cells. Proc Natl Acad Sci U S A *107*, 11906-11911.

Meyer, M., Hols, A.K., Liersch, B., Leistner, R., Gellert, K., Schalke, B., Marx, A., and Niedobitek, G. (2011). Lack of evidence for Epstein-Barr virus infection in myasthenia gravis thymus. Ann Neurol *70*, 515-518.

Stefanoff, C.G., Hassan, R., Gonzalez, A.C., Andrade, L.A., Tabak, D.G., Romano, S., and Zalcberg, I.R. (2003). Laboratory strategies for efficient handling of paraffin-embedded tissues for molecular detection of clonality in non-hodgkin lymphomas. Diagn Mol Pathol *12*, 79-87.

van Dongen, J.J., Langerak, A.W., Bruggemann, M., Evans, P.A., Hummel, M., Lavender, F.L., Delabesse, E., Davi, F., Schuuring, E., Garcia-Sanz, R.*, et al.* (2003). Design and standardization of PCR primers and protocols for detection of clonal immunoglobulin and T-cell receptor gene recombinations in suspect lymphoproliferations: report of the BIOMED-2 Concerted Action BMH4-CT98-3936. Leukemia *17*, 2257-2317.